Available online at www.sciencedirect.com
SCIENCE DIRECT®
Journal of volcanology and geothermal research
ELSEVIER
Journal of Volcanology and Geothermal Research 129 (2004) 155–172
www.elsevier.com/locate/jvolgeores

Experimental study on the effects of crustal temperature and composition on assimilation with fractional crystallization at the floor of magma chambers

Katsuya Kaneko [a,*], Takehiro Koyaguch [b]

[a] *Graduate School of Human and Environmental Studies, Kyoto University, Sakyo-ku, Kyoto 606-8501, Japan*
[b] *Earthquake Research Institute, University of Tokyo, 1-1-1 Yayoi, Tokyo 113-0032, Japan*

Received 2 July 2002; received in revised form 18 January 2003; accepted 25 January 2003

Abstract

When a hot basaltic magma is emplaced into continental crust or a pre-existing silicic magma chamber, the processes of assimilation with fractional crystallization (AFC) are likely to control the liquid line of descent of the magma. These processes are particularly important at the floor of the magma chamber because evolved light liquids generated by floor melting readily mix with the overlying basaltic magma. In order to clarify the effects of temperature and composition of the floor on the AFC processes, we experimentally investigated simultaneous melting and crystallization of a NH_4Cl–H_2O binary eutectic system. In the experiments, evolution of temperature and compositional profiles of a hot solution overlying a cold solid mixture of variable initial temperatures and compositions were measured. The initial NH_4Cl concentrations of solid and liquid are chosen to be higher than the eutectic composition, such that the density change of the experimental material by crystallization and melting is qualitatively the same as that of natural magmas and crusts. The results show that a mushy layer forms at the floor due to simultaneous crystallization and (partial) melting and that the liquid evolves due to mixing with liquids released by crystallization and melting. The ratio of melting mass to crystallization mass (M/C ratio) depends on the initial floor temperature and composition. As the initial floor temperature decreases, the rate of melting largely decreases, so that the M/C ratio becomes smaller. As the initial NH_4Cl concentration of the solid floor decreases, the degree of partial melting of the floor increases; however, it does not necessarily result in an increase in the M/C ratio. The higher melt fraction of the mushy layer increases permeability within the mushy layer, so that vertical exchange between the liquid in the mushy layer and the more concentrated overlying liquid is enhanced. This effect promotes crystallization in the mushy layer, and decreases the M/C ratio. It is suggested that the M/C ratio during AFC processes depends on details of the mixing process in the liquid layer such as spacing and meandering of buoyant plumes.

Keywords: magma chamber; assimilation with fractional crystallization; fluid dynamic experiment; simultaneous melting and crystallization; compositional convection

* Corresponding author. Tel.: +81-75-753-6874; Fax: +81-75-753-6872.
E-mail addresses: katsuya@gaia.h.kyoto-u.ac.jp (K. Kaneko), tak@eri.u-tokyo.ac.jp (T. Koyaguch).

0377-0273/03/$ – see front matter © 2003 Elsevier B.V. All rights reserved.
doi:10.1016/S0377-0273(03)00238-5

1. Introduction

Recent geochemical studies show that assimilation with fractional crystallization (AFC) is one of the most important processes that account for the diversity of volcanic and other igneous rocks (e.g. De Paolo, 1981; Spera and Bohrson, 2001). Despite the petrological importance, the mass and heat transfer during the AFC processes has not been fully investigated from the viewpoint of physics. One of the key problems is to specify the physical parameters which govern the relative contributions of fractional crystallization and assimilation. When a set of geochemical data from a certain petrological suite is given, we may be able to estimate the proportion of fractional crystallization to assimilation on the basis of mass balance. However, in order to predict the geological conditions from those geochemical data, we must know the physics which determines the proportion of the two effects. In this study we investigate some possible controlling factors using fluid dynamic experiments.

Fluid dynamical considerations suggest that melting and crystallization at the floor of the magma chamber are expected to be of particular importance in the AFC processes. Generally, liquids generated by melting of continental crusts are lighter than a basaltic magma. Therefore, evolved liquids generated by partial melting and/or crystallization at the floor rise up and readily mix into the basaltic magma, which significantly affects subsequent crystallization and the liquid line of descent (e.g. Tait and Jaupart, 1989, 1992; Huppert, 1989; Woods, 1991; Magirl and Incropera, 1993; Kerr, 1994a,b; Koyaguchi and Kaneko, 1999; Kaneko and Koyaguchi, 2000). On the other hand, liquids generated by melting at the roof do not affect the compositional differentiation of the basalt, because they form a separate liquid layer over the basaltic magma (Campbell and Turner, 1987; Huppert and Sparks, 1988; Kaneko and Koyaguchi, 2000).

The significance of mixing of the evolved liquid generated by floor melting is supported by some geological observations, particularly by those from silicic–mafic layered intrusions. Silicic pipes which have roots in silicic rock and penetrate overlying mafic rock have been reported from many silicic–mafic layered intrusions (e.g. Chapman and Rhodes, 1992; Wiebe, 1994, 1996) (Fig. 1a). These observations indicate that new basalt replenished a silicic magma chamber with solidifying crystal mush at the floor and ponded at the boundary between the mush and the overlying silicic magma (Fig. 1b), and that the evolved liquids generated by melting of silicic mush at the floor mixed with the overlying basaltic magma (Fig. 1d). In these situations, the AFC processes in the basaltic magma are a natural consequence, because fractional crystallization due to cooling is inevitably accompanied by mixing with the

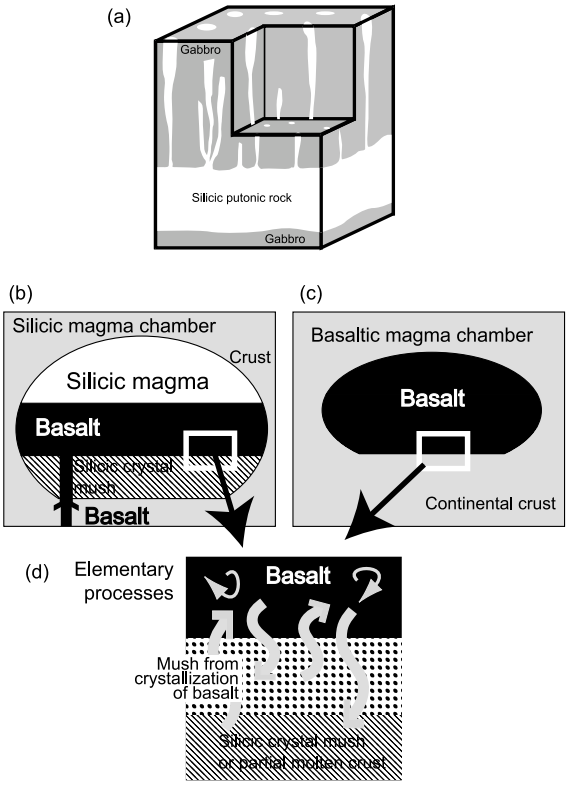

Fig. 1. (a) Schematic sketch showing contact relationships between gabbros and silicic plutonic rock in a mafic–silicic layered intrusion (after Capman and Rhodes, 1992). Silicic pipes have roots in the silicic plutonic rock and penetrate the overlying gabbro. (b) Schematic sketch of AFC at the floor of a mafic–silicic zoned magma chamber. (c) Basaltic magma chamber in a continental crust. (d) Buoyant interstitial liquids in the floor rise and mix with the overlying basalt resulting from situations (b) and (c).

evolved liquids from the floor. Although field evidence for floor melting is not always clear for other geological situations, simultaneous melting and crystallization at the floor would be one of the possible mechanisms which account for the AFC processes in magma chambers.

When melting and crystallization occur simultaneously at the floor of a magma chamber, there are at least two parameters that can control the AFC processes in addition to the characteristics of the magma itself; those are the temperature and composition of the floor. When a basaltic magma replenishes a silicic magma chamber and ponds over the silicic mush like the examples of silicic–mafic layered intrusions (Fig. 1b), the floor is already heated up and partially molten. In such cases, considerable amount of evolved liquid would be supplied from the floor to the basalt. On the other hand, when a basalt is intruded into a cold continental crust (Fig. 1c), the effect of floor melting would become limited before the basalt is largely crystallized (Bergantz, 1989; Bergantz and Dawes, 1994). The chemical composition of the floor is another important factor controlling the effects of assimilation, because the degree of partial melting for a given temperature largely depends on the chemical composition. Thus, we focus on effects of the initial temperature and composition of the floor on the relative effects of fractional crystallization and assimilation.

In this study we carried out a series of fluid dynamic experiments involving simultaneous melting and crystallization at the floor using aqueous solutions. In the experiments, the initial temperature and composition of the floor were systematically changed. Although there are some theoretical and experimental models of crystallization and/or melting in multicomponent systems in engineering and science fields (e.g. Bennon and Incropera, 1987; Huppert and Sparks, 1988; Worster, 1991; Bergantz, 1992; Diepers et al., 1999), no generalized model which covers the condition where simultaneous melting and crystallization occur at the floor has been established. Particularly, as far as we know, no previous experiments have been designed to investigate the effects of the initial temperature and composition of the floor on the AFC processes. We, therefore, attempt to capture the essence of these complex phenomena as the first step in this preliminary report, rather than to propose a quantitative model.

2. Experimental method

We carried out experiments in which a hot liquid layer was in contact with a cold solid layer at the floor level. We used a hot solution and cold solid mixtures within a NH_4Cl–H_2O binary eutectic system (Fig. 2a). The liquid used in all experiments was 28 wt% NH_4Cl aqueous solution at its saturation temperature (23.5°C). To ascertain the effects of the solid composition on the evolution of the system, the cold solid mixtures used in Exps. 1–3 had compositions of the eutectic (19.7 wt% NH_4Cl), 28 wt% NH_4Cl, and 73 wt% NH_4Cl, respectively, and the initial temperature was −16°C, slightly lower than the eutectic temperature of −15.4°C (Fig. 2a). To ascertain the effects of the solid temperature, a fourth experiment using a cold (−44°C) solid mixture of eutectic composition was carried out (Fig. 2a). The solid with eutectic composition (Exps. 1 and 4) completely melted at the eutectic temperature, while the solids with 28 and 73 wt% NH_4Cl (Exps. 2 and 3) partially melted, forming eutectic liquids which left 10 wt% and 66 wt% residual NH_4Cl solids at the eutectic temperature, respectively. For a solid of given composition (more concentrated in NH_4Cl than the eutectic), the solid starts to (partially) melt at the eutectic temperature and produces eutectic melt. As the degree of partial melting increases beyond that of the eutectic fraction, the temperature must increase and the melt becomes denser as it is enriched in NH_4Cl. For a liquid of given composition (more concentrated in NH_4Cl than the eutectic), as crystallization proceeds along the liquidus curve, the liquid becomes less dense as it is depleted in NH_4Cl. The variation of the density of released liquid/melt with the degree of crystallization/partial melting in this system is qualitatively the same as it is in the basaltic magma-continental crust system.

A schematic sketch of the apparatus used in

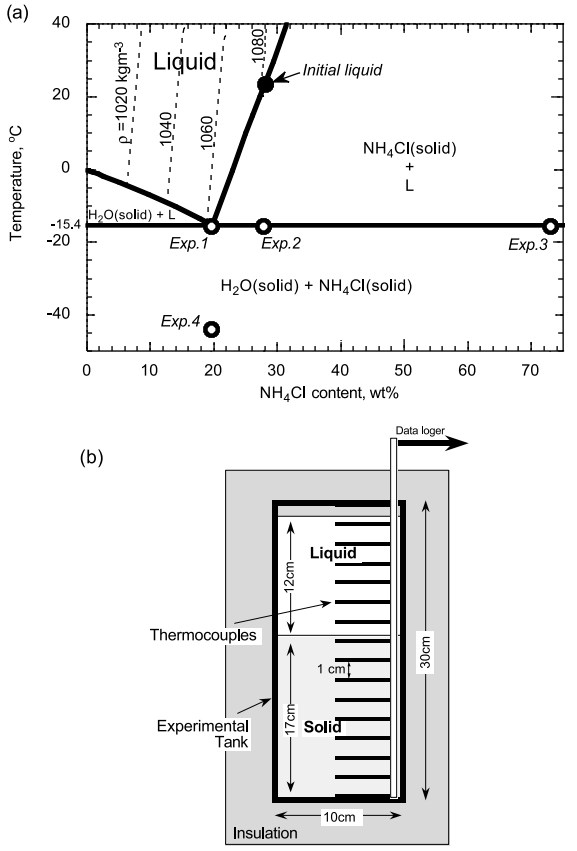

Fig. 2. (a) The phase diagram of the NH_4Cl–H_2O binary eutectic system and the initial condition of the experiments. The eutectic temperature and composition are −15.4°C and 19.7 wt%. The solid lines show the liquidus and solidus, and the dashed lines show the iso-density contours of the solution (kg m^{-3}). The filled circle shows the initial liquid conditions in all experiments, and the open circles show the initial conditions of the solids in Exps. 1–4. (b) Schematic sketch of the experimental apparatus.

our experiments is presented in Fig. 2b. Before the run, a solid mixture 17 cm thick was created in the lower half of a Perspex experimental tank with inner dimensions of $10\times10\times30$ cm high. We could make a homogeneous initial solid mixture with the eutectic composition simply by cooling a liquid with the eutectic composition. A solid mixture with 28 wt% NH_4Cl was made by repeatedly quenching a thin liquid layer (1–2 mm deep) with 28 wt% NH_4Cl in a strongly cooled tank (<-40°C) in order to avoid fractionation during solidification. A solid mixture with 73 wt% NH_4Cl was made by rapidly cooling a mixture of NH_4Cl crystals (diameter <0.5 mm) and saturated NH_4Cl aqueous solution. In this case, fractionation due to convection during solidification is limited by large solid fraction (about 60 vol%). Homogeneity of the initial solid mixtures made by these methods was tested in additional experiments. A hot aqueous solution 12 cm deep was rapidly (within 20 s) poured into the experimental tank, and then the run started. During this process, the surface of the solid was covered with thin foam plastic to avoid erosion. Each side of the tank was thermally insulated from the laboratory with foam plastic 5 cm thick. The liquid was dyed in order to observe mixing with the generated melt. The vertical temperature profile was measured by an array of Alumel–Chromel thermocouples, the junctions of which were placed near the center of the experimental tank at heights fixed at 1-cm vertical intervals. Liquid samples were periodically withdrawn from 4 or 5 levels and their refractive indices were measured, allowing deduction of the concentration of solute to ±0.2 wt%.

3. Outline of the experimental results

The qualitative features of the fluid convection were similar in all experiments. As soon as each experiment started, a mushy layer developed between the liquid and solid layers due to crystallization of the NH_4Cl from the liquid and the boundary between the solid and mushy layers moved downwards due to melting (Fig. 3a). When the solid had the eutectic composition (Exps. 1 and 4), the solid melted uniformly and the mushy layer formed only due to the crystallization of the liquid. On the other hand, when the composition of the solid was not eutectic (Exps. 2 and 3), the mushy layer developed as a consequence of both partial melting of the solid and crystallization from the liquid. In the latter cases, the dyed liquid penetrated to a level below the original solid/liquid interface at a much higher rate than would be expected by diffusion alone. This indicates convective exchange between the interstitial liquid of the partially molten solid layer and the overlying liquid. The melt generated

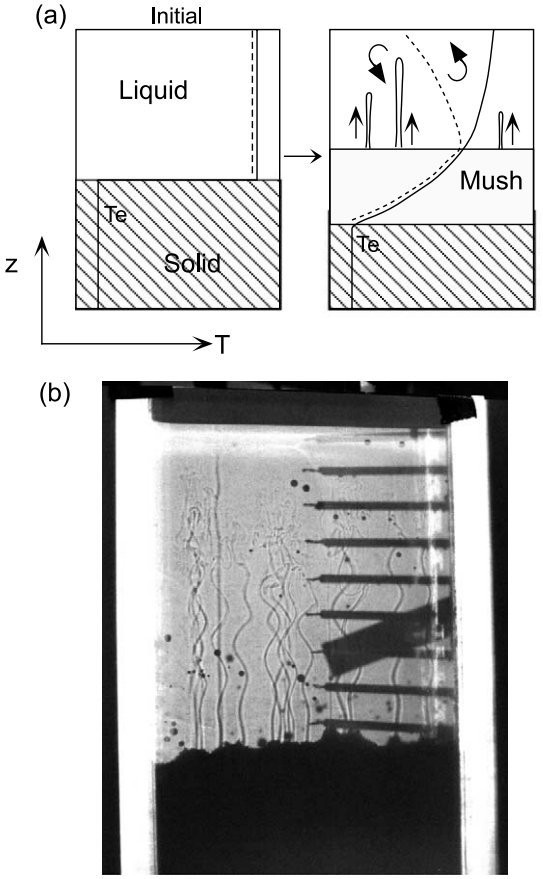

Fig. 3. (a) Schematic sketch of temperature and compositional profiles of each experiment. The solid lines show temperature profiles. The dashed lines show liquidus temperature profiles determined by liquid compositions. T_e is the eutectic temperature. (b) A photograph (shadowgraph) of Exp. 2 at 120 min.

at the floor and the interstitial liquid in the mushy layer were lighter than the main part of the liquid and rose in plumes, driving compositional convection in the liquid layer (Fig. 3a,b). Many chimneys, through which less dense liquid was channeled, formed in the mushy layer. Diameters of the chimneys were about 1 mm. In the early stage of the run, convection was very vigorous. Many narrowly spaced plumes meandered, causing them to collide and become entangled. The temperature and composition were almost uniform throughout the liquid layer above the mushy layer due to the vigorous convection at this stage. Subsequently, convection became less vigorous. The plumes spaced more widely and their number decreased. The plumes meandered but collided rarely. At this stage, stabilizing gradients in temperature and composition became apparent within the liquid layer; temperature increased upward and NH_4Cl concentration decreased upward (Fig. 3a). As a result, the liquid layer was everywhere at a temperature above the liquidus (Fig. 3a), and it did not carry NH_4Cl crystals. From the data on temperature and liquid composition it is inferred that the crystallization continued within the mushy layer. The average NH_4Cl concentration in the liquid layer decreased with time due to mixing with the plumes containing a low NH_4Cl concentration.

The evolution of the temperature profiles in the mushy and liquid layers did not vary between different runs except for the temperature profile near the solid/mush interface (Fig. 4a). The migration rate of the solid/mush interface in each experiment was close to the rate predicted in a case where there is no fluid motion and melting and crystallization at the floor are driven only by thermal conduction (referred to as the 'pure-conduction' case hereafter) (Fig. 4b). The model in the pure-conduction case is an extension of the theoretical model of crystallization in a binary eutectic system by Worster (1986), where the effects of melting are additionally taken into account. These results indicate that heat transfer is basically governed by heat conduction and that compositional convection carries a low heat flux (cf. Tait and Jaupart, 1989, 1992; Kaneko and Koyaguchi, 2000).

4. Quantitative features

4.1. Ratio of melting mass to crystallization mass

Some quantitative features of mass and heat transfer, such as positions of liquid/mush and mush/solid interfaces, the compositions of the liquid layer, the melting and crystallization masses are given as a function of time in Fig. 4b–e. The melting and crystallization masses can be evaluated from the positions of the solid/mush and mush/liquid interfaces, the temperature in the

mushy layer, and the average NH_4Cl concentration of the liquid layer on the basis of mass balance and phase relationships (Appendix A). In each experiment, both the melting and crystallization masses increase with time (Fig. 4d,e). The crystallization mass rapidly increases just after the run started, because the initial saturated liquid is suddenly cooled by the cold floor. On the basis of these melting and crystallization masses, we can obtain the ratio of the melting mass to the crystallization mass (hereafter we call this ratio the M/C ratio); the M/C ratio tends to have a small value in the early stage because of the initial burst of crystallization and subsequently reaches a constant value (or slightly increases with time) in each experiment (Fig. 5). The evolutions of melting and crystallization masses and the M/C ratio systematically change with the initial solid condition. Among all these quantities, variations in the M/C ratio are of particular interest from the viewpoint of petrogenesis involving AFC processes (e.g. De Paolo, 1981). We will describe how the M/C ratio changes as a function of the initial solid temperature and composition below.

The effect of the initial solid temperature is straightforward. As the initial temperature of the solid increases, the M/C ratio becomes larger (Exps. 1 and 4 in Fig. 5). The migration rates of the solid/mush interface and the melting rates are more rapid in the warmer solid (Exp. 1) than the colder solid (Exp. 4) (see Fig. 4b,d), and the in-

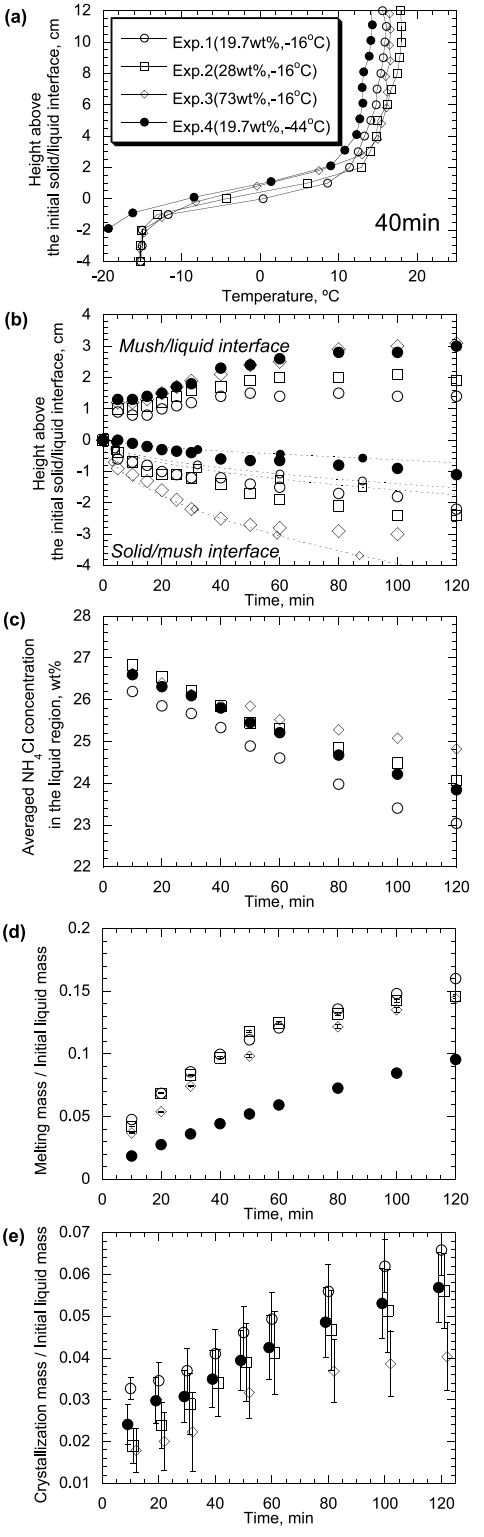

Fig. 4. The experimental results. The open circles, squares, and diamonds, and the filled circles indicate data obtained from Exps. 1, 2, 3, and 4, respectively. Exp. 1: the initial composition of the solid (C_{S0}) = 19.7 wt% NH_4Cl (the eutectic composition), the initial temperature of the solid (T_{S0}) = −16°C; Exp. 2: C_{S0} = 28 wt% NH_4Cl, T_{S0} = −16°C; Exp. 3: C_{S0} = 73 wt% NH_4Cl, T_{S0} = −16°C; Exp. 4: C_{S0} = 19.7 wt% NH_4Cl, T_{S0} = −44°C. (a) Temperature profiles at 40 min. (b) The positions of the solid/mush and mush/liquid interfaces as a function of time. The dashed lines denote the evolution predicted in the 'pure-conduction' case. (c) The average NH_4Cl concentration of the liquid layer as a function of time. (d) The melting mass normalized by the initial liquid mass as a function of time. (e) The crystallization mass normalized by the initial liquid mass as a function of time. The bars in (d) and (e) show the possible ranges of the values (see Appendix A).

tensity of compositional convection increases due to larger generation rate of buoyant melt. This is simply because less heat is needed to heat a warmer solid to the eutectic temperature and then to melt it in such a way that the melting mass increases. Unless compositional convection is very strong, the compositional convection does not carry significant heat flux (cf. Tait and Jaupart, 1989; Kaneko and Koyaguchi, 2000) and so the effect of the initial solid temperature on the temperature profile within the liquid and mushy layers is limited (see Fig. 4a). Although crystallization rate slightly increases as the initial temperature increases due to compositional convection between the mushy and liquid layers (this effect will be discussed later), the variation in crystallization rate in the liquid and mushy layers is insignificant compared with the variation in melting rate at the solid/mush interface. Consequently, the M/C ratio increases as the initial temperature of the solid increases.

The results in Fig. 5 show that the M/C ratio systematically decreases as the initial NH_4Cl concentration of the solid decreases (Exps. 1–3). The direction of the change in the M/C ratio is opposite to what is expected from the degree of partial melting (i.e. the M/C ratio decreases as the degree of partial melting of the solid increases). As mentioned above, the heat flux due to compositional convection is insignificant. Therefore, there is little difference in melting rate among Exps. 1–3 (Fig. 4d). On the other hand, the crystallization rate decreases as the initial NH_4Cl concentration of the solid increases (Fig. 4e). The variation of the crystallization rate is explained primarily by the variation in efficiency of compositional exchange between the liquid and mushy layers. Crystallization in the mushy layer is driven by exchange between the high NH_4Cl liquid in the lower part of the liquid layer and the low NH_4Cl interstitial liquid in the mushy layer. Therefore, the crystallization rate in the mushy layer is affected by compositional profile as well as average composition in the liquid layer.

Fig. 6 shows temperature and composition profiles at the time a given melting mass was reached (the mass of generated melt normalized by the initial liquid mass $\sim$0.11). The liquid composition is expressed by the corresponding liquidus temperature in this diagram; the liquidus temperature increases with the NH_4Cl concentration (see Fig. 2a). The NH_4Cl concentration in the liquid layer decreases upward in each experiment, and the average NH_4Cl concentration in the liquid layer decreases as the initial NH_4Cl concentration of the solid decreases. These compositional profiles indicate that most of the light eutectic liquid generated by melting passed through the liquid layer as plumes without efficient mixing with the ambient liquid and ponded at the top of the liquid layer. This is consistent with the qualitative observation that the rising plumes meandered but rarely collided (Fig. 3b). When the mixing within the liquid layer is limited, the crystallization in the mushy layer is enhanced as the exchange of the liquid between the mushy layer and the lower part of the liquid layer becomes more efficient. Within the range of experimental conditions, as the initial NH_4Cl concentration of the solid decreases, the degree of partial melting of the solid floor at the eutectic temperature increases (Fig. 2a), and the mushy layer becomes more permeable (the permeability in the mushy layer is dominantly con-

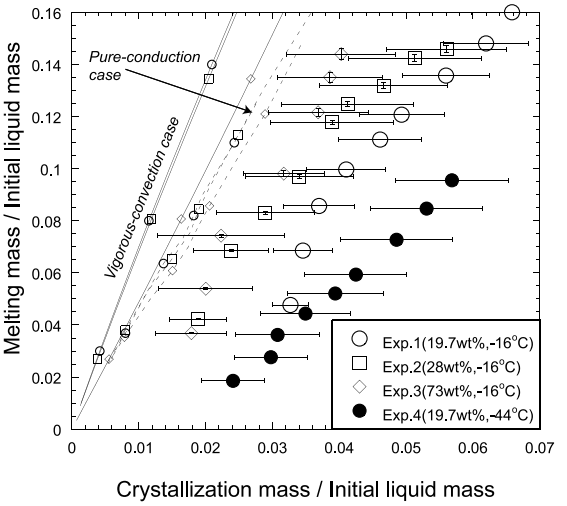

Fig. 5. Melting mass vs. crystallization mass in the experiments. Numerical results of the 'pure-conduction' case (dashed line) and the 'vigorous-convection' case (solid lines) under the same conditions as Exps. 1, 2, and 3 are also shown. The masses are normalized such that the initial liquid mass is unity. The bars show the possible ranges of the values (see Appendix A).

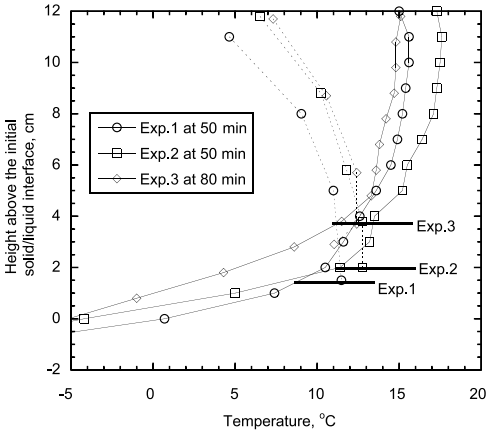

Fig. 6. Temperature and liquidus temperature profiles at the time when the melting masses (melting mass/initial liquid mass) reached ~0.11. For Exp. 1 the profile at 50 min, for Exp. 2 the profile at 50 min, and for Exp. 3 the profile at 80 min are shown. The solid lines show temperatures and the dashed lines show liquidus temperatures determined by liquid compositions. The thick solid lines show the mush/liquid interface.

trolled by the amount of residual NH_4Cl crystals), which increases the number of plumes and enhances the exchange of the liquid between the mushy layer and the lower part of the liquid layer. Consequently, the crystallization rate increases and the M/C ratio decreases with the decreasing initial NH_4Cl concentration of the solid.

It should be noted that this relationship between the M/C ratio and the intensity of compositional convection holds only for the cases where plumes passed through the liquid layer without efficient mixing. As the liquid layer is homogenized by vigorous convection, the NH_4Cl concentration of liquid supplied from the liquid layer to the mushy layer (i.e. that of the lower part of the liquid layer) decreases, which can reduce the crystallization in the mushy layer and hence increases the M/C ratio. In Fig. 5 numerical results of crystallization and melting masses for two extreme cases of convective intensity are shown. One is the case where there is no fluid motion and heat transfer is limited by pure conduction (i.e. the 'pure-conduction' case in Fig. 4b). The other is the case in which the convection is vigorous enough for the region above the solid floor (including the mushy layer) to be perfectly homogenized in temperature and composition (referred to as the 'vigorous-convection' case hereafter). In the vigorous-convection case, we assume that the migration rate of the liquid/solid boundary is in a quasi-steady state as:

$$\dot{a} = F_T/\rho[C_p(T-T_{S0}) + L\phi(T)] \quad (1)$$

where $\dot{a}$ is the migration rate of the liquid/solid boundary, F_T is the heat flux from the liquid to the liquid/solid boundary, ρ is the density, C_p is the specific heat, L is the latent heat, T and T_{S0} are the liquid and initial solid temperatures, and $\phi(T)$ is the melt fraction of the partially-molten floor at T (Huppert and Sparks, 1988). The M/C ratios in both the pure-conduction and vigorous-convection cases are larger than those of the experiments where the intensity of convection is intermediate between the two extreme cases.

In summary, it is concluded that compositional convection has two distinct effects; those are 'exchange' and 'mixing'. 'Exchange' means that lighter and denser liquids exchange their vertical positions and 'mixing' means that the liquid layer is homogenized by stirring. These two effects play opposite roles in determining the M/C ratio. Exchange promotes the supply of NH_4Cl from the lower part of the liquid layer to the mushy layer, which reduces the M/C ratio. On the other hand, mixing decreases the NH_4Cl concentration of the lower part of the liquid layer, and so increases the M/C ratio. From the fact that the M/C ratios in the experiments are smaller than the two extreme cases of 'pure-conduction' and 'vigorous-convection' (Fig. 5) it is inferred that the relationship between the M/C ratio and the intensity of con-

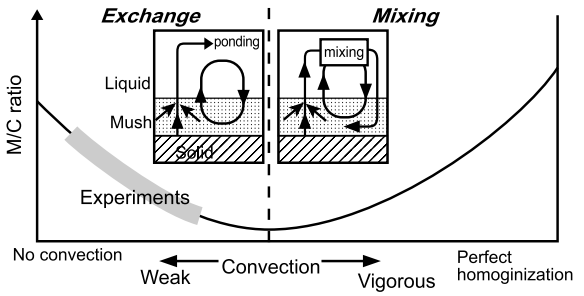

Fig. 7. Schematic diagram on the M/C ratio change against the intensity of convection.

vection is as shown in Fig. 7, where the M/C ratio goes through a minimum between the two end-members. The end-members define two regimes. When the intensity of compositional convection is relatively low, exchange plays a predominant role. As a result, the M/C ratio decreases as the compositional convection becomes more intensive (exchange regime in Fig. 7). As convection becomes even more vigorous, the effect of mixing (homogenization) becomes more important than that of exchange. Consequently, the M/C ratio can increase with the intensity of convection (mixing regime in Fig. 7).

4.2. Degree of mixing

The above consideration suggests that the degree of mixing in the liquid layer due to the compositional convection is an important factor that controls the M/C ratio. In this subsection, we quantitatively estimate the degree of mixing in the liquid layer on the basis of the criterion by Jellinek et al. (1999). We compare the present experimental results with the previous results by Jellinek et al. (1999) in which no crystallization occurs and no mushy layer forms at the floor.

Jellinek et al. (1999) introduced the efficiency of the convective mixing as:

$$E = \frac{P_e - P_{\min}}{P_{\max} - P_{\max}} \tag{2}$$

Here P_e, $P_{\max}$, and $P_{\min}$ are evaluated by:

$$P = \int_{h_b}^{h_t} g[\rho_a - \rho(z)]z dz \tag{3}$$

where h_b and h_t are the heights of the bottom and top of the liquid, respectively, ρ_a is the density of the ambient liquid, and $\rho(z)$ is the density profile in the liquid layer, and g is the gravitational acceleration. P_e is estimated by substituting the observed density profile into $\rho(z)$ in Eq. 3, while $P_{\max}$ and $P_{\min}$ are estimated by substituting the density profiles in the cases of complete mixing (i.e. uniform $\rho(z)$) and no mixing (i.e. stepwise $\rho(z)$ where the light fluid overlies the dense one), respectively.

The quantity E is based on the idea that convection is a process where the gravitational potential energy of buoyant liquid is converted into the kinetic energy of rising plumes. Some of the kinetic energy is used to do the mechanical work of mixing while the remaining kinetic energy is dissipated as a result of viscous stresses. The proportion of potential energy used for mixing depends on the interaction between the ambient liquid and the ascending buoyant liquid. In the extreme case of no mixing buoyant plumes pass through the ambient liquid layer without much kinetic energy building up in the ambient liquid. In this case, a stepwise density profile forms and $P_e = P_{\min}$ so that $E = 0$. In the opposite extreme case of complete mixing, a maximum amount of the initial gravitational potential energy is retained in the uniform density profile, so that $P_e = P_{\max}$ and $E = 1$.

Jellinek et al. (1999) found that the mixing efficiency, E, depends on two key parameters in the cases where a compositionally buoyant fluid was injected into an overlying liquid layer and no crystallization occurred (inset in Fig. 8): a Reynolds number based on the thickness of the liquid layer:

$$Re \approx \frac{B^{1/3} h^{4/3}}{\nu_a} \tag{4}$$

and the ratio:

$$U = \nu_a / \nu_i \tag{5}$$

of the ambient liquid kinetic viscosity to the plume liquid kinetic viscosity. Here ν_a and ν_i are the kinetic viscosities of the ambient and plume liquids, respectively, h is the thickness of the liquid layer, and $B = gV_i(\rho_a - \rho_i)/\rho_a$ is the buoyancy flux from the boundary, where V_i is the flux per unit area of plume liquid, and ρ_a and ρ_i are the densities of the ambient and plume liquids.

Fig. 8 shows the relationship between Re and E in the present experiments. We can calculate B and hence Re from the observed experimental data (the compositional profile in the liquid layer, the changing rate of the liquid composition, and the liquid layer thickness). On the other hand, we cannot determine the value of E directly from the experimental data, because the composition of the rising plumes was not directly measured in the experiments. We estimate possible ranges of E

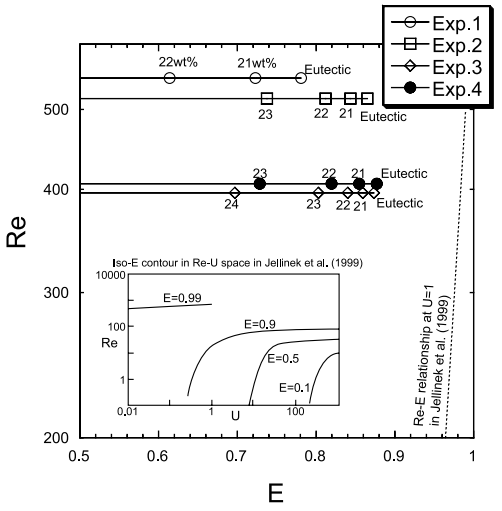

Fig. 8. Relationship between Reynolds number (*Re*) and mixing efficiency (*E*) in the experiments at 100 min. Open circles: Exp. 1, open squares: Exp. 2, open diamonds: Exp. 3, and filled circles: Exp. 4. Because the composition of the rising plumes was not directly measured in the experiments, we estimate *E* for various assumed NH_4Cl concentrations of the plumes. The assumed NH_4Cl concentrations are labeled near the symbols. Because the NH_4Cl concentration of the plume must be greater than the eutectic composition, the value of *E* for the eutectic composition provides the upper bound of *E* for each experiment. The small diagram is a contour map illustrating how *E* varies in *Re*–*U* space on the basis of the experiments without crystallization (Jellinek et al., 1999). Here *U* represents the viscosity ratio of ambient and plume liquids. The dashed line is the relationship between *Re* and *E* for $U=1$ (i.e. viscosity ratio in the present experiments) by Jellinek et al. (1999). See text for details.

for assumed NH_4Cl concentrations of the plumes (greater than the eutectic composition). The value of *E* decreases with increasing assumed NH_4Cl concentrations. The results show that the values of *Re* based on Eq. 4 range from 400 to 550 in the present experiments. *Re* increases as the initial temperature of the solid increases (Exps. 1 and 4) or the initial NH_4Cl concentration of the solid decreases (Exps. 1–3). The values of *Re* tend to be higher in the experiment where more intensive convection was observed. This is because the value of *Re* is mainly determined by buoyancy flux of the rising plumes, *B* (see Eq. 4), which is expected to increase with the intensity of the compositional convection. The value of *E* ranges from 0.5 to 0.9 depending on assumed plume composition for each experiment. Because NH_4Cl concentrations of plumes are never less than that of the eutectic composition, the value of *E* for each experiment would not exceed the maximum value shown in Fig. 8.

Fig. 8 also graphs the relationship between *E* and *Re* based on the experimental results by Jellinek et al. (1999). According to their results, inefficient mixing with $E<0.9$ is possible only when the ambient fluid is more viscous than the plume (i.e. $U>1$) and convection is weak ($Re<10^2$) (inset in Fig. 8). For the same conditions as our experimental conditions (i.e. $U=1$ and $Re>10^2$), their analysis predicts almost complete homogenization; *E* increases from 0.98 to 0.99 with the increasing *Re* from 400 to 550 (Fig. 8). This implies that the mixing is substantially less efficient in the present experiments than those by Jellinek et al. (1999) particularly for the higher *Re* experiments (e.g. Exp. 1). The difference in mixing efficiency between the two series of experiments is attributed to crystallization and formation of the mushy layer at the floor. The qualitative observations of the present and previous experiments suggest that mixing is promoted by collision between rising plumes. When no crystallization occurs at the floor, the spacing of plumes is narrow and the plumes undergo meandering instabilities, which cause them to collide and become entangled (Jellinek et al., 1999). Consequently, efficient mixing between the plumes and the ambient liquid results. On the other hand, when the mushy layer forms at the base like the present experiments, plume spacing is controlled by chimney spacing in the mushy layer which is generally much wider than the plume spacing in the case without the mushy layer. In such cases, most of the plumes do not collide each other, and the lighter liquids in the plumes pass through the ambient denser liquids without efficient mixing (Fig. 3b). As a result, a stable density stratification forms.

The above comparisons between our experimental results and those by Jellinek et al. (1999) suggest that mixing in the liquid layer is largely suppressed by the presence of a mushy layer at the bottom. This effect plays an essential role when the liquid composition evolves in 'exchange' regime in Fig. 7. Because a mushy layer inevitably

forms accompanied by crystallization of magma and partial melting of crust, the effect should be taken into account in considering the AFC processes in natural systems.

5. Petrological implications

When a basaltic magma is emplaced into a preheated continental crust, crystallization of the basaltic magma and melting of the surrounding crust simultaneously occur in the magma chamber. A similar process may occur when a basaltic magma replenishes a mushy silicic magma chamber. In those cases the liquid line of descent of the basaltic magma must be controlled by the combined effects of fractional crystallization and assimilation of melted crustal materials, namely AFC processes. A number of petrological and geochemical works reveal that compositional variations of volcanic and plutonic rocks in many igneous provinces can be explained by AFC processes. Assuming compositions of parental magma and assimilated crust and distribution coefficients of chemical species, a possible range of M/C ratios can be estimated from the chemical variations of the natural samples (e.g. De Paolo, 1981). According to recent geochemical studies, M/C ratios range from 0.1 to 0.5 in most cases, although there are a few cases with high M/C ratios (up to 1) in intermediate-silicic rocks from island-arc or continental volcanic regions (Table 1). There is no systematic correlation between the M/C ratio and compositions of the assimilants. In this section we attempt to assess these values of M/C ratio from the viewpoint of the present results.

Before applying the present experimental results to natural examples, we estimate the M/C ratios in the two extreme cases, the 'vigorous-convection' and 'pure-conduction' cases, for natural magma-crust systems. Judging from the present results, the M/C ratios for these extreme cases are considered to represent an upper bound of the possible range of M/C ratio (e.g. Fig. 5). We consider a situation where a horizontal layer of hot basaltic magma with a certain thickness in contact with a layer of cold crust with very large thickness. We can obtain M/C ratios as a function of time by calculating mass and heat transfer ac-

Table 1
Recent studies on estimation of M/C ratios in the AFC process

Rock generated by AFC process	Parental magma	Assimilant	M/C ratio	Reference
Granite in Alpine pluton	Basalt	Granitoid	0.2	Bigazzi et al. (1986)
Granite in Sierra Nevada	Basalt	Pelitic rock	0.4	Davies and Tommasini (2000)
Granodiorite–granite in the Central European Hercynides	Partial melt of metabasite	Paragneiss	0.5	Janoušek et al. (2000)
Andesite–rhyolite in arc volcano	Basalt	Granulite or granitoid	0.3–0.4, 0.6–0.8, and 0.5–0.6 in 3 units	Caffe et al. (2002)
Granodiorite in Proterozoic terrain	Basalt	Metasediment	0.17–0.25	Barbey et al. (2001)
Andesite in arc volcano	Basalt	Lower crust	0.9	Kobayashi and Nakamura (2001)
Andesite in arc volcano	Basalt	Granite	0.04–0.05	Bourdon et al. (2002)
Basaltic andesite–rhyolite in continental rift	Basalt	Granitoid	0.8–0.9 and 0.2–0.3 in 2 units	Grunder (1992)
Basalt and andesite–rhyolite in volcanism with opening of Atlantic Ocean	Basalt	Leucogranite	0.25 (basalt) and 0.4 (felsic)	Kirstein et al. (2000)
Continental flood basalt	Basalt	Upper continental crust	0.25	Carlson et al. (1981)
Basic dyke in continental flood basalt	Basalt	Continental crust	0.25	Ellam et al. (1998)
Alkali basalt in oceanic island basalt	Alkali basalt	Oceanic crust	0.15–0.23	Caroff et al. (1999)
Tholeiitic basalt in hotspot	Picrite	Iceladic andesite–dacite	0.25	Eiler et al. (2000)

companied by simultaneous melting and crystallization for the above two extreme cases. Because the temporal changes of M/C ratio are small in each calculation (it tends to slightly increase with time in a warm crust and decrease with time in a cold crust), we adopt the maximum M/C ratios as representative values and show them as a function of the initial temperatures of the crusts in Fig. 9a. The effects of a variation in solid composition are taken into account by changing relationships between melt fraction and temperature. Simplified relationships between melt fraction and temperature for gabbroic, tonalitic and granitic crusts are assumed on the basis of previous compilations of melting relations of hydrous crustal materials (Fig. 9b). Those relationships can be approximated by that of a eutectic system (e.g. Wyllie, 1977; Bergantz, 1989; Koyaguchi and Kaneko, 1999), and so they are similar to the present experimental conditions in this sense.

In both cases the maximum M/C ratio increases from <0.1 to 3 as the initial temperatures of the crusts increase from 100 to 700°C (Fig. 9a). The M/C ratio of the 'pure-conduction' case is substantially smaller than that of the 'vigorous-convection' case at low temperatures, whereas the M/C ratios of the two cases converge at high crustal temperatures. This is because the larger fraction of heat is used for heating up the colder crust before melting in the pure-conduction case. Fig. 9a also shows that there is a weak dependence on the composition of the crust; a more mafic crust gives the smaller maximum M/C ratio. This compositional dependence can be explained by the fact that the degree of partial melting at a given temperature is smaller as the crustal composition becomes more mafic. The results of Fig. 9a and the relatively low values of M/C ratio in the natural system (<0.5 in most cases; see Table 1) indicate that magmas were emplaced into a rather cold (100–300°C) crust, if the melting and crystallization in the two extreme cases are assumed. However, present experimental results provide us another explanation. The experimental results suggest that the M/C ratio depends on the manner of convection as well as the initial floor temperature and composition; M/C ratio can be smaller than those of the two extreme cases when the

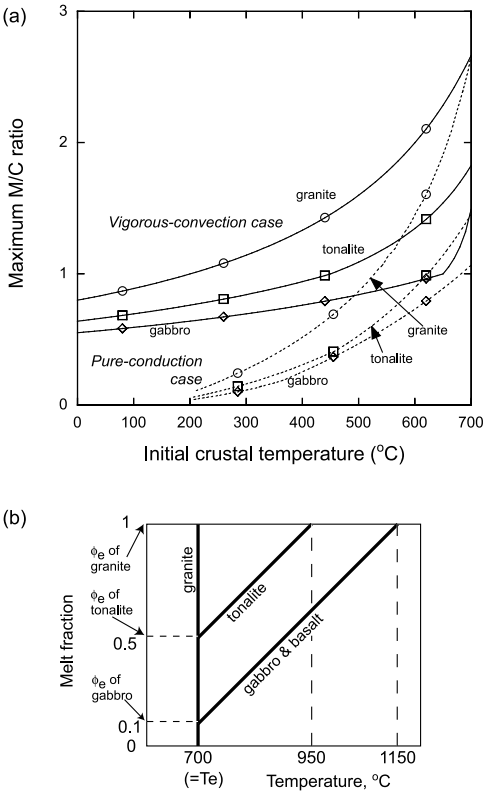

Fig. 9. Estimation of the M/C ratio for natural basalt-crust systems. (a) The maximum M/C ratio for the two extreme cases (the 'vigorous-convection' and 'pure-conduction' cases in Fig. 5) is shown as a function of initial crustal temperature. Solid curves show the results of the 'vigorous-convection' case, and dashed curves show the results of the 'pure-conduction' case. The calculations are carried out for three types of crusts: granite (circle), tonalite (square), and gabbro (diamond). The parameter values used in the calculations are listed in Table 2. (b) The relationships between melt fraction and temperature for these crustal materials are given on the basis of those of typical hydrous magmas and crusts (Robertson and Wyllie, 1971; Wyllie, 1971, 1977; Bergantz, 1989; Koyaguchi and Kaneko, 1999). It is assumed that all the types of crust have a common eutectic temperature ($Te = 700$°C); gabbro and tonalite melt up to melt fractions (ϕ_e) of 0.1 and 0.5 at the eutectic temperature, respectively, and the melt fractions increase with increasing temperature at the rate of 0.002°C^{-1}, while granite melts completely at the eutectic temperature. It is assumed that basaltic magma has the same relationships between melt fraction and temperature as gabbro and an initial temperature of 1150°C.

compositional convection results in 'exchange' of the light and dense fluids rather than 'mixing' of the two fluids (Fig. 7). Because of this effect, the M/C ratio can decrease as the degree of partial

Table 2
Parameter values of the NH_4Cl–H_2O system and a typical magma system

Symbol	NH_4Cl–H_2O system	Typical magma system	Unit
κ	1.7×10^{-7}	8×10^{-7}	$m^2\ s^{-1}$
Cp	3.4×10^{3}	1×10^{3}	$J\ kg^{-1}\ K^{-1}$
L	3.0×10^{5}	3×10^{5}	$J\ kg^{-1}$
μ	1.0×10^{-3}	10^{2}–10^{3}	Pa s
α	1.7×10^{-4}	5×10^{-5}	K^{-1}
D	2.0×10^{-9}	10^{-12}	$m^2\ s^{-1}$
ρ	1.0×10^{3}	2.7×10^{3}	$kg\ m^{-3}$
ΔT	39	5×10^{2}	K
$\rho\gamma\Delta C$	20	10^{2}	$kg\ m^{-3}$
$\rho\beta\Delta C$	27	10^{2}	$kg\ m^{-3}$

melting of the solid floor at a given temperature increases. The small values of the M/C ratio in the natural systems are accounted for by the melting-crystallization process where 'exchange' plays a dominant role in convection in a hot crust. The compositional dependence observed in the experimental results may also rationalize the observation that the M/C ratio tends to be relatively high in some examples where a mafic lower crust is involved as an assimilant.

Finally we briefly discuss the limitations of the present model. The experimental and natural magma systems are different in some respects, such as dimensions and viscosities of liquids. In order to apply our experimental results to natural magma systems, similarity between the experimental and natural systems in their dynamic context is examined on the basis of comparison of dimensionless parameters in Appendix B. The magnitudes of dimensionless numbers that determine the convection regimes in the liquid layer (i.e. Ra_C or Re; see Appendix B for their definitions) depend on the thickness of magma layers. For a basaltic intrusion of 10 m thick, the porous, thermal, and compositional Rayleigh numbers (Ra_P, Ra_T, and Ra_C) are 10^1, 10^9, and 10^9, respectively, and the Reynolds number is less than 10^1. Those values are less than or similar to those of our experimental system (Table 3). The relationships that the M/C ratio decreases with the increasing degree of partial melting of the floor (i.e. those like Fig. 5) would be observed in those thin intrusions. Such basaltic layers are commonly observed in mafic–silicic layered intrusions (e.g. Chapman and Rhodes, 1992; Wiebe, 1996). For a basaltic intrusion of 1 km, Ra_C exceeds 10^{15} and

Table 3
Values of dimensionless numbers

Dimensionless number	Experimental system	Magma system		
		10 m thick	100 m thick	1 km thick
Ra_P	$>10^3$	10^1–10^2	10^2–10^3	10^3–10^4
Ra_T	10^9	10^9–10^{10}	10^{12}–10^{13}	10^{15}–10^{16}
Ra_C	10^9	10^9–10^{10}	10^{12}–10^{13}	10^{15}–10^{16}
Pr	5	10^5–10^6	10^5–10^6	10^5–10^6
σ	2	0.6	0.6	0.6
Le	10^2	10^6	10^6	10^6
Re (Eq. 4)	10^2–10^3	10^0–10^1	10^1–10^2	$\sim10^3$

Permeabilities for estimation of the Porous Rayleigh numbers are calculated with the equation for permeable media with chimneys (Tait and Jaupart (1992), equation B7) for the experimental system (porosity >0.7, chimney radius = 0.5 mm) and with the Kozeny–Carman equation for the magma systems (porosity = 0.6, crystal diameter = 1–5 mm). Physical parameters in Table 2 are used. Re for the magma system is based on Jellinek and Kerr, 1999.

Re is 10^3 (Table 3). Those values are greater than or similar to those of the present experimental system. The mixing due to compositional convection may play a more important role than the experimental system in such thick intrusions. Unfortunately, no petrological data which support the relationship between the dimension and the geochemical features (i.e. M/C ratio) of the intrusion are available at present.

In conclusion, the experimental results and a simple scaling analysis suggest that the M/C ratio in the AFC processes of basaltic magma in magma chambers within continental crusts changes as a function of the initial floor temperature and composition. Although the petrological implication of the experimental results is still qualitative, it is suggested that the AFC processes depend on the regime of compositional convection (i.e. 'exchange' or 'mixing'). It is notable that the M/C ratio can decrease as the degree of partial melting of the floor increases, when mixing due to compositional convection is inefficient. In order to quantitatively evaluate the possible range of M/C ratio in various magma-crust systems and to predict the liquid line of descent due to the AFC processes as a function of geophysical and/or geological parameters, further experimental and theoretical studies as well as field observations are necessary. In particular, efficiency of mixing due to compositional convection (e.g. Jellinek et al., 1999a) would be the key problem. More rigorous models on mass and heat transfer in a mushy layer (e.g. Worster, 1991, 1997; Chen, 1995; Shulze and Worster, 1998) that predict spacing of chimneys and plumes are also required. Field observations on dimensions of basaltic intrusions and mafic–silicic layered intrusions and those on zoned magma chambers would provide important constraints on this problem.

Acknowledgements

We thank Michael Manga, Ross Kerr, and Alison Leitch for helpful comments on the manuscript. K.K. was supported by JSPS Fellowships for Japanese Junior Scientists.

Appendix A. Estimation of melting and crystallization masses in the experiments

Melting mass (M_f) and crystallization mass (M_x) can be estimated from the experimental results on the basis of mass balance and phase relationships. Consider a situation where a liquid with initial mass M_0 and composition C_0 is in contact with a solid with composition C_S (Fig. A1). When a certain mass (M_S) of the solid partially melts, conservation of mass is expressed as:

$$M_0 + M_S = M_l + M_m \tag{A1}$$

and conservation of NH_4Cl content is given by:

$$M_0 C_0 + M_S C_S = M_l C_l + M_m C_m \tag{A2}$$

where M_l and M_m are the masses of the liquid layer and the mushy layer, respectively, and C_l and C_m are the average compositions (mass fraction of NH_4Cl) of liquid layer and the average bulk composition of the mushy layer, respectively. Because M_0, M_S, and M_l are available from the position of liquid/mush and mush/solid boundaries and the densities of the solid and liquid layers, and C_0 and C_S are known, the mass and bulk composition of the mushy layer (i.e. M_m and C_m) in Eqs. A1 and A2 can be determined by measuring the average composition in the liquid layer (C_1).

Because mush is composed of crystals and liquid, M_m is expressed as the sum of masses of crystals (M_{mx}) and liquid (M_{ml}) as:

$$M_m = M_{mx} + M_{ml} \tag{A3}$$

The crystals in the mushy layer originated from

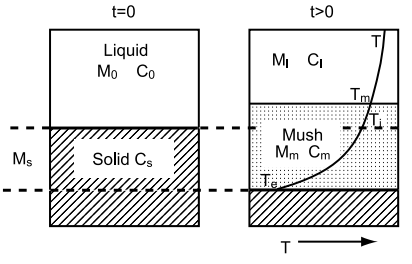

Fig. A1. Schematic reference diagram for the estimation of the melting and crystallization masses. Solid curve in the mushy and liquid layers shows the temperature profile.

partial melting and crystallization. Therefore, M_{mx} is expressed as:

$$M_{mx} = M_x + M_r \tag{A4}$$

where M_r is the mass of residual crystals in partial melting, and M_x is the mass of precipitated crystals from the liquid (i.e. crystallization mass). By definition melting mass is expressed as:

$$M_f = M_S - M_r \tag{A5}$$

Melting mass (M_f) and crystallization mass (M_x) are estimated from M_{mx} and M_r using Eqs. A4 and A5.

In order to estimate M_{mx} and M_r in Eqs. A4 and A5 we need to know the temperature and compositional profiles within the mushy layer, which we could not measure in the experiments. Accordingly, we determine only the upper and lower bounds of these quantities on the basis of phase relationship and available data. From mass balance within the mushy layer, we obtain:

$$C_m M_m = C_x M_{mx} + \overline{C}_{ml} M_{ml} \tag{A6}$$

where C_x is the composition of the crystal ($C_x = 1$ for NH_4Cl crystal) and $\overline{C}_{ml}$ is the average liquid composition within the mushy layer. It is assumed that the liquid composition within the mushy layer at a given position, C_{ml}, varies along the liquidus curve, and so it is given as:

$$C_{ml}(T) = C_e + (T - T_e)/\Gamma \tag{A7}$$

where C_e is the eutectic composition, T_e is the eutectic temperature, and Γ is the liquidus slope that has approximately a constant value (see Fig. 2a). Because the maximum and minimum temperatures in the mushy layer are those at the mush/liquid interface (T_m) and the solid/mush interface (T_e), we can deduce the range of $\overline{C}_{ml}$ as

$$C_e \le \overline{C}_{ml} \le C_{ml}(T_m). \tag{A8}$$

From Eqs. A3 and A6 and Inequality (Eq. A8), the upper and lower bounds of M_{mx} are estimated as:

$$M_{\max}^{\min} \equiv \frac{C_m - C_{ml}(T_m)}{C_x - C_{ml}(Tm)} M_m \le M_{mx} \le M_{mx}^{\max} \equiv \frac{C_m - C_e}{C_x - C_e} M_m. \tag{A9}$$

On the other hand, the upper and lower bounds of M_r are estimated from the two extreme cases; those are the case where partial melting of the solid occurs at the eutectic temperature (T_e) and the case where partial melting proceeds up to the temperature at the original solid/liquid interface measured in the experiments (T_i) without compositional change of the mushy layer. From the phase relationship, the range of M_r is given by:

$$M_r^{\min} \equiv \frac{C_s - C_{ml}(T_i)}{C_x - C_{ml}(T_i)} M_S \le M_r \le M_r^{\max} \equiv \frac{C_S - C_e}{C_x - C_e} M_S \tag{A10}$$

Finally, from Eqs. A4 and A5 we obtain the range of M_x and M_f:

$$M_{mx}^{\min} - M_r^{\max} \le M_x \le M_{mx}^{\max} - M_r^{\min} \tag{A11}$$

and:

$$M_S - M_r^{\max} \le M_f \le M_S - M_r^{\min}. \tag{A12}$$

The results of Fig. 4d,e are obtained from M_f and M_x, respectively.

Appendix B. Similarity analyses for the experimental and natural systems

In order to apply our experimental results to the natural magma system, we should consider similarity between the experimental and natural systems in their dynamic context on the basis of comparison of dimensionless numbers in the conservation equations of mass, energy, and momentum. Because the present problem depends on the fluid dynamics in both the liquid and mushy layers, both the regions must be considered. In the following assessment, six dimensionless parameters that may govern the phenomena, as well as *Re* (Eq. 4), are used following Tait and Jaupart (1992). It is assumed that the mushy layer is ideal in the sense that the solid and liquid phases are in perfect, local thermodynamic equilibrium and that the solid forms a stationary rigid matrix, whose permeability is locally isotropic and a function only of the local melt fraction. Although the detailed physics of crystallization

and melting such as crystallization kinetics within the mushy layer is taken into account in some sophisticated models (e.g. Diepers et al., 1999), there is much experimental evidence that many real mushy layers conform closely to an ideal mushy layer (Worster, 1997), and it is unlikely that such kinetic effects significantly modify the qualitative features of the present conclusion (e.g. those of Fig. 7).

Assuming that the liquidus relationship between the temperature and concentration is linear and that the liquid is Boussinesq, the equations summarized by Tait and Jaupart (1992) were made dimensionless using the following scales:

Length	H
Time	κ/H^2
Mass	$\rho_0 H^3$
Temperature	$\Delta T = T_0 - T_e$
Composition	$\Delta C = C_0 - C_e$
Permeability	Π_0

where H is the layer thickness, κ is the thermal diffusion coefficient, ρ_0 is the density, T_0 and C_0 are the initial temperature and composition of the liquid, T_e and C_e are the eutectic temperature and composition, and Π_0 is the representative permeability. Six dimensionless parameters appear:

Porous Rayleigh number	$Ra_P = \dfrac{g\gamma\Delta T H \Pi_0}{\kappa\nu}$
Thermal Rayleigh number	$Ra_T = \dfrac{g\alpha\Delta T H^3}{\kappa\nu}$
Compositional Rayleigh number	$Ra_C = \dfrac{g\beta\Delta C H^3}{\kappa\nu}$
Prandtl number	$Pr = \dfrac{\nu}{\kappa}$
Stefan number	$\sigma = \dfrac{L}{C_P \Delta T}$
Lewis number	$Le = \dfrac{\kappa}{D}$

where α and β are the thermal and compositional expansion coefficients of the liquid, respectively, γ is the thermal expansion coefficient of the saturated solution, D is the compositional diffusivity, L is the latent heat of fusion, and C_P is the specific heat.

Typical values of these dimensionless parameters for the experimental and magma systems are presented in Table 3. Because of large difference in viscosity between magma and NH_4Cl solution, Prandtl number (Pr) is substantially different between the experimental and magma systems. In the case of thermal convection, it is known that the difference in Pr will have little effects on the convection regime under very large Rayleigh number conditions (Krishnamurti, 1970). When the basaltic magma is more than 10 m thick, the Rayleigh numbers in the experimental and magma systems are sufficiently large (Fig. B1; Table 3). If those results of thermal convection are applicable to the present case of double diffusive convection, we can conclude that the thermal and compositional evolution observed in the experiments simulates certain natural magma systems at least in a qualitative sense. On the other hand, according to a recent experimental study on mixing by natural convection (Jellinek et al., 1999), the flow pattern in the liquid layer may critically depend on the Reynolds number (Re; see Eq. 4). In this case the experimental system would apply to the thicker (up to 1-km-thick) basaltic layer (Table 3). We must wait for further experimental and theoretical

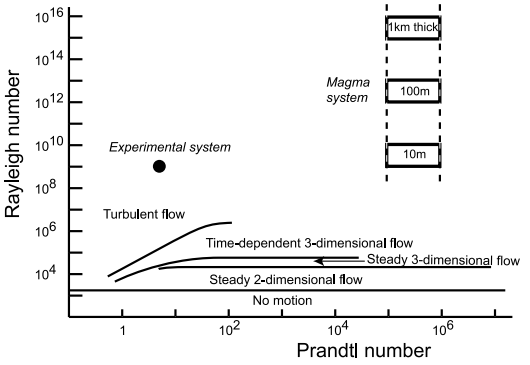

Fig. B1. Diagram showing the positions of the experimental and magma systems in Rayleigh number–Prandtl number space. The boundaries of convection regimes are based on the experimental results of thermal convection in a horizontal fluid layer (Krishnamurti, 1970). In the present case, both the compositional and thermal gradients drive convection, and so two Rayleigh numbers (Ra_T and Ra_C) are defined. Because the compositional effect is larger than the thermal one (the ratio of the density change due to compositional change to that due to temperature change ($\beta\Delta C/\alpha\Delta C$) is about 4 in the experimental system and about 2 in the magma system), it is assumed that Ra_C roughly represents the Rayleigh number in this diagram.

studies in order to determine whether Rayleigh number or Reynolds number plays an essential role in this issue.

References

Barbey, P., Nachit, H., Pons, J., 2001. Magma-host interactions during differentiation and emplacement of a shallow-level, zoned granitic pluton (Tarçouate pluton, Morocco): Implications for magma emplacement. Lithos 58, 125–143.

Bennon, W.D., Incropera, F.P., 1987. A continuum model for momentum, heat and species transport in binary solid-liquid phase change, I. Model formulation. Int. J. Heat Mass Transf. 30, 2161–2170.

Bergantz, G.W., 1989. Underplating and partial melting: Implications for melt generation and extraction. Science 245, 1093–1095.

Bergantz, G.W., 1992. Conjugate solidification and melting in multicomponent open and closed systems. Int. J. Heat Mass Transf. 35, 533–543.

Bergantz, G.W., Dawes, R., 1994. Aspects of magma generation and ascent in continental lithosphere. In: Ryan, M.P. (Ed.), Magmatic Systems. Academic Press, London, pp 291–317.

Bigazzi, G., Del Moro, A., Macera, P., 1986. A quantitative approach to trace element and Sr isotope evolution in the Adamello Batholith (Northern Italy). Contrib. Mineral. Petrol. 94, 46–53.

Bourdon, E., Eissen, J.-P., Monzier, M., Robin, C., Martin, H., Cotten, J., Hall, M.L., 2002. Adakite-like lavas from Antisana volcano (Ecuador): Evidence for slab melt metasomatism beneath the Andean Northern Volcanic Zone. J. Petrol. 43, 199–217.

Caffe, P.J., Trumbull, R.B., Coira, B.L., Romer, R.L., 2002. Petrogenesis of Early Neogene magmatism in the Northern Puna: Implications for magma genesis and crustal processes in the Central Andean Plateau. J. Petrol. 43, 907–942.

Campbell, I.H., Turner, J.S., 1987. A laboratory investigation of assimilation at the top of a basaltic magma chamber. J. Geol. 95, 155–172.

Carlson, R.W., Lugmair, G.W., Macdougall, J.D., 1981. Columbia River volcanism: The question of mantle heterogeneity or crustal contamination. Geochim. Cosmochim. Acta 45, 2843–2949.

Caroff, M., Guillou, H., Lamiaux, M., Maury, R.C., Guille, G., Cotten, J., 1999. Assimilation of ocean crust by hawaiitic and mugearitic magmas: An example from Eiao (Marquesas). Lithos 46, 235–258.

Chapman, M., Rhodes, J.M., 1992. Composite layering in the Isle au Haut Igneous Complex, Maine: Evidence for periodic invasion of a mafic magma into an evolving magma reservoir. J. Volcanol. Geotherm. Res. 51, 41–60.

Chen, C.F., 1995. Experimental study of convection in a mushy layer during directional solidification. J. Fluid Mech. 293, 81–98.

Davies, G.R., Tommasini, S., 2000. Isotopic disequilibrium during rapid crustal anatexis: Implications for petrogenetic studies of magmatic processes. Chem. Geol. 162, 169–191.

De Paolo, D.J., 1981. Trace element and isotopic effects of combined wall rock assimilation and fractional crystallization. Earth Planet. Sci. Lett. 53, 189–202.

Diepers, H.J., Bechermann, C., Steinbach, I., 1999. Simulation of convection and ripening in a binary alloy mush using the phase-field method. Acta Mater. 47, 3663–3678.

Eiler, J.M., Grönvold, K., Kitchen, N., 2000. Oxygen isotope evidence for the origin of chemical variations in lavas from Theistareykir volcano in Iceland's northern volcanic zone. Earth Planet. Sci. Lett. 184, 269–286.

Ellam, R.M., Upton, B.G.J., Fitton, J.G., 1998. Petrogenesis of late stage magmatism at Hold with Hope, East Greenland. Contrib. Mineral. Petrol. 133, 51–59.

Grunder, A.L., 1992. Two-stage contamination during crustal assimilation: Isotopic evidence from volcanic rocks in eastern Nevada. Contrib. Mineral. Petrol. 112, 219–229.

Huppert, H.E., 1989. Phase changes following the initiation of a hot turbulent flow over a cold solid surface. J. Fluid Mech. 198, 293–319.

Huppert, H.E., Sparks, R.S.J., 1988. The generation of granitic magmas by intrusion of basalt into continental crust. J. Petrol. 29, 599–624.

Janoušek, V., Bowes, D.R., Rogers, G., Farrow, C.M., Jelínek, E., 2000. Modelling divers processes in the petrogenesis of a composite batholith: The Central Bohemian Pluton, Central European Hercynides. J. Petrol. 41, 511–543.

Jellinek, A.M., Kerr, R.C., Griffiths, R.W., 1999. Mixing and compositional stratification produced by natural convection, 1. Experiments and their application to Earth's core and mantle. J. Geophys. Res. 104, 7183–7201.

Jellinek, A.M., Kerr, R.C., 1999. Mixing and compositional stratification produced by natural convection, 2. Application to the differentiation of basaltic and silicic magma chambers and komatiite lava flows. J. Geophys. Res. 104, 7203–7218.

Kaneko, K., Koyaguchi, T., 2000. Simultaneous crystallization and melting at both the roof and floor of crustal magma chambers: Experimental study using NH_4Cl-H_2O binary eutectic system. J. Volcanol. Geotherm. Res. 96, 161–174.

Kerr, R.C., 1994a. Melting driven by vigorous compositional convection. J. Fluid Mech. 280, 255–285.

Kerr, R.C., 1994b. Dissolving driven by vigorous compositional convection. J. Fluid Mech. 280, 286–301.

Kirstein, L.A., Peate, D.W., Hawkesworth, C.J., Turner, S.P., Harris, C., Mantovani, M.S.M., 2000. Early Cretaceous basaltic and rhyolitic magmatism in Southern Uruguay associated with the opening of the South Atlantic. J. Petrol. 41, 1413–1438.

Kobayashi, K., Nakamura, E., 2001. Geochemical evolution of Akagi volcano, NE Japan: Implications for interaction between island-arc magma and lower crust, and generation of isotopically various magmas. J. Petrol. 42, 2303–2331.

Koyaguchi, T., Kaneko, K., 1999. A two-stage thermal evolution model of magmas in continental crust. J. Petrol. 40, 241–254.

Krishnamurti, R., 1970. On the transition to turbulent convection. J. Fluid Mech. 42, 295–320.

Magirl, C.S., Incropera, F.P., 1993. Flow and morphological conditions associated with unidirectional solidification of aqueous ammonium chloride. Trans. ASME 115, 1036–1043.

Robertson, J.K., Wyllie, P.J., 1971. Rock-water systems, with special reference to the water-deficient region. Am. J. Sci. 271, 252–277.

Shulze, T.P., Worster, M.G., 1998. A numerical investigation of steady convection in mushy layers during the directional solidification of binary alloy. J. Fluid Mech. 356, 199–220.

Spera, F.J., Bohrson, W.A., 2001. Energy-constrained open-system magmatic Processes, I. General model and energy-constrained assimilation and fractional crystallization (EC–AFC) formulation. J. Petrol. 42, 999–1018.

Tait, S., Jaupart, C., 1989. Compositional convection in viscous melts. Nature 338, 571–574.

Tait, S., Jaupart, C., 1992. Compositional convection in a reactive crystalline mush and melt differentiation. J. Geophys. Res. 97, 6735–6756.

Wiebe, R.A., 1994. Silicic magma chambers as traps for basaltic magmas: The Cadillac Mountain intrusive complex, Mount Desert Island, Maine. J. Geol. 102, 423–437.

Wiebe, R.A., 1996. Mafic–silicic layered intrusions: The role of basaltic injections on magmatic processes and the evolution of silicic magma chambers. Trans. R. Soc. Edinb. (Earth Sci.) 87, 233–242.

Woods, A.W., 1991. Fluid mixing during melting. Phys. Fluids A 3, 1393–1404.

Worster, M.G., 1986. Solidification of an alloy from a cooled boundary. J. Fluid Mech. 167, 481–501.

Worster, M.G., 1991. Natural convection in a mushy layer. J. Fluid Mech. 224, 335–359.

Worster, M.G., 1997. Convection in mushy layers. Annu. Rev. Fluid Mech. 29, 91–122.

Wyllie, P.J., 1971. The Dynamic Earth. Wiley, Chicester, NY.

Wyllie, P.J., 1977. Crustal anatexis: An experimental review. Tectonophysics 43, 41–71.